

# RE-VISITING RHIC SNAKES AND SPIN ORBIT\*

F. Méot, R. Gupta, H. Huang, A. Marusic, V. Ranjbar, G. Robert-Demolaize  
BNL, Upton, NY, USA

## Abstract

Recent analyses of RHIC run12 to run15 proton-carbon polarimeter measurements have shown significant tilt of the polarization vector from vertical, at high energy essentially. This is confirmed by extensive measurements performed in the present Run 17. Possible origins of such large tilt may reside in snake spin rotation angle or orbit defects, to mention just two. Dedicated simulations have been undertaken to investigate possible causes, they are presented and discussed, they include the computation and use of 3-D field maps of RHIC siberian snakes.

## INTRODUCTION

This study is motivated by the observation - at high energy mostly - of a significant off-vertical tilt of the stable spin precession direction at the pC CNI polarimeter, in both Blue and Yellow RHIC rings [1]. On the other hand, the numerical simulations undertaken provide, beyond these spin tilt investigations, additional material and data regarding RHIC optics and polarization, based on the use of snake field maps.

## POLARIZED BEAMS AT RHIC

The Relativistic Heavy Ion Collider (RHIC) Blue and Yellow rings are injected by the source-linac-booster-AGS chain (Fig. 1). The collider accelerates and stores ions or polarized proton beams [2], the latter from 23.8 GeV injection energy ( $G\gamma = 45.5$  in spin standards -  $G=1.792847$  is the anomalous magnetic moment,  $\gamma$  is the Lorentz relativistic factor) up to 100 GeV ( $G\gamma = 191$ ) or 255 GeV ( $G\gamma = 487$ ) for about 8 hour stores. Beams collide at STAR (IP6) and PHENIX (IP8) detectors.

Proton beam polarization is maintained in each one of the two RHIC rings by of a pair of diametrically opposed helical dipole assemblies ("Full Siberian Snakes" in Fig. 1, each ensures 100% ( $180^\circ$ ) spin rotation).

## SNAKE FIELD MAPS

RHIC snake [3] is comprised of four identical, 2.4 m effective length, 360 degree right-handed twisted helix modules (Fig. 2). Two are low-field and sit at both ends (maximum on-axis field denoted  $B_{\text{low}}$  in the text, common current  $I_{\text{low}}$ ), a high-field pair sits in between (maximum on-axis field denoted  $B_{\text{high}}$  in the text, common current  $I_{\text{high}}$ ), the magnetic field vector at the ends of the snake is vertical.

## Theory

These newly computed OPERA maps have been subject to various comparisons with basic theoretical expectations [4-

\* Work supported by Brookhaven Science Associates, LLC under Contract No. DE-AC02-98CH10886 with the U.S. Department of Energy.

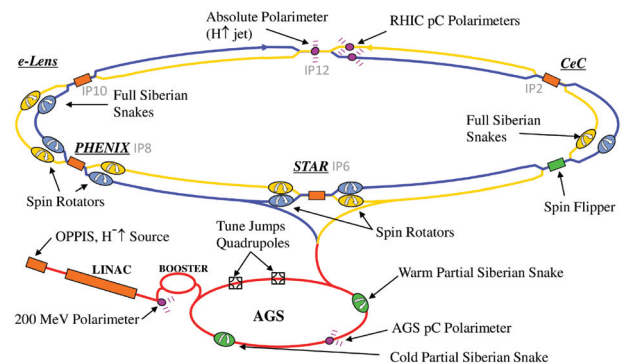


Figure 1: RHIC collider and its injector chain.



Figure 2: OPERA view of one 2.4 m,  $360^\circ$ -twist helix module of the 10.5 m long, 4-module RHIC snake.

7] and with earlier RHIC snake studies [8,9], based on ray-tracing [10], as follows.

- The transverse field components along the helical trajectory (ignoring end field fall-off effects) satisfy, to order zero in  $x$ ,  $y$  excursions (respectively, the horizontal and vertical distance to the helix axis) (Fig. 3),

$$\begin{cases} B_x = B_0 \cos(ks) \\ B_y = B_0 \sin(ks) \end{cases} \quad (1)$$

with  $k = 2\pi/\lambda$  the helical coil pitch (here,  $\lambda = 2.4$  m,  $k = 2.618 \text{ m}^{-1}$ ),  $s$  the distance along the helix axis,  $B_0$  the peak transverse field value.

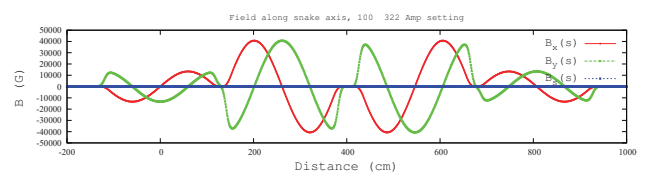


Figure 3: Field along the snake axis in the OPERA model. Extreme on-axis field values come out to be, in the low-field helix module  $|\vec{B}| = 1.340$  T, in the high-field helix module  $|\vec{B}| = 3.903$  T.

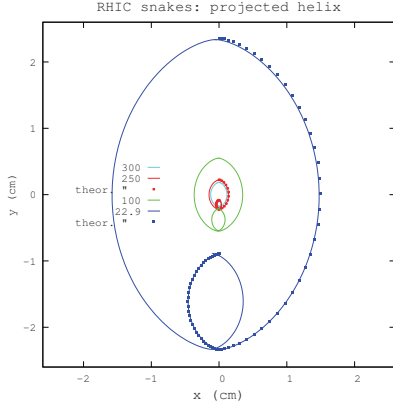


Figure 4: Projection of the (non-circular) helical motion in the transverse plane (smaller excursion is in the low-field magnet), from theory at 22.9 and 250 GeV (solid lines, Eq. 3) and from ray-tracing in the OPERA field maps at 23, 100, 250 and 300 GeV (markers).

To second order in  $x, y$ ,

$$\begin{cases} B_x/B_0 = \cos(ks)(1 + \frac{k^2}{8}(3x^2 + y^2)) + \frac{k^2}{4}xy \sin(ks) \\ B_y/B_0 = \sin(ks)(1 + \frac{k^2}{8}(x^2 + 3y^2)) + \frac{k^2}{4}xy \cos(ks) \\ B_l/B_0 = -k(x \sin(ks) - y \cos(ks)) \end{cases} \quad (2)$$

Given the radial excursions of concern here, namely  $x, y$  in 2 cm range at lower energy (see Fig. 4), while  $k^2/8 \approx 1$ , the non-linear terms have negligible contribution to the field.

- The particle motion is a non-circular helix (Fig. 4) with coordinates (taking the origin at  $s = 0$ )

$$\begin{cases} x = x_0 + \frac{B_0}{k^2 B \rho} [\cos(ks) - 1] \\ y = y_0 + \frac{B_0}{k^2 B \rho} \sin(ks) - \frac{B_0}{k B \rho} s \end{cases} \quad (3)$$

with  $x_0, x'_0, y_0, y'_0$  the initial coordinates,  $\alpha$  the angle of the field to the vertical at entrance ( $\alpha = 0$  here),  $B\rho$  the particle rigidity. The vertical amplitude of the motion over the extent  $\lambda$  of an helical dipole is

$$\Delta y = \frac{B_0 \lambda}{k B \rho} \quad (4)$$

- Trajectory lengthening can be derived from Eqs. 3 with appropriate approximations, and writes

$$\Delta s = \frac{\lambda^3}{2\pi^2} \frac{B_{low}^2 + B_{high}^2}{B\rho^2} = \frac{\lambda^3 c^2}{2\pi^2 M} \frac{B_{low}^2 + B_{high}^2}{\gamma^2 - 1} \quad (5)$$

with  $M = 938.272 \times 10^6 \text{ eV}/c^2$  the particle mass and  $\gamma$  its Lorentz relativistic factor,  $c$  the velocity of light. Trajectory lengthening shows in Fig. 4, energy dependence and comparison with ray-tracing outcomes are shown Fig. 5.

- The vertical orbit offset at entrance of the snake, necessary to center the helical trajectory on the high-field helix axis, is approximately

$$y_{off} \approx \frac{1}{2} \Delta y_{high} - \Delta y_{low} = \frac{B_{high} - 2B_{low}}{2k B \rho} \lambda \quad (6)$$

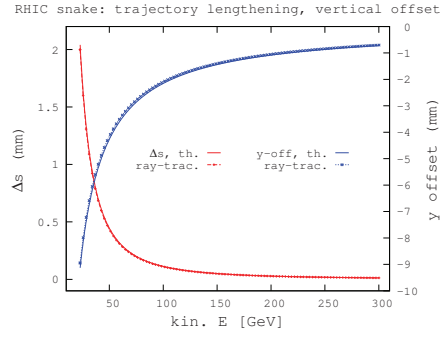


Figure 5: Energy dependence of the orbit lengthening (left vertical axis) and vertical orbit off-centering at snake entrance (right), from theory (solid lines, Eqs. 5 and 6, respectively) and from ray-tracing.

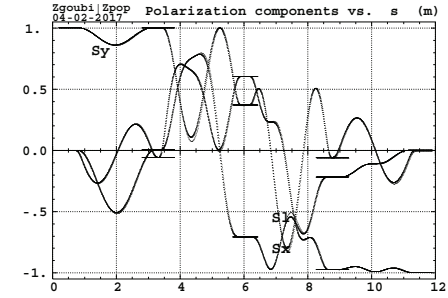


Figure 6: Evolution of the spin components along the helical trajectories. Four energies are represented : 23, 100, 250 and 300 GeV, they superimpose.

with  $\Delta y_{hi}, \Delta y_{low}$  the elevation in respectively the high- and low-field helix (Eq. 3, Fig. 4). This energy dependence is displayed in Fig. 5.

- The spin transport matrix  $[M_{ij}]$  through the snake provides the spin rotation angle

$$\mu = \text{acos}((\text{Trace}(M) - 1)/2)$$

and spin rotation axis

$$(a_s, a_x, a_y) = (M_{32} - M_{23}, M_{13} - M_{31}, M_{21} - M_{12})$$

It is obtained by tracking three initially orthogonal polarization conditions along the reference on-momentum path (Fig. 6). In the ring case this also provides the spin tune  $Q_s = \mu / 2\pi$  [10].

## SPIN ROTATION

The spin rotation angle  $\mu$  and spin precession axis orientation  $\phi$  are sketched in Fig. 7. Figure 8 displays a scan of their dependence in energy over the range 23-300 GeV (the helical trajectory has been maintained centered on the axis in the high-field helix modules (as in Fig. 4) at all currents over that energy scan).

The required 180deg/45deg spin rotation parameters in the 250 GeV region is obtained with optimal maximum

fields  $B_{low} = 1.26 T$ ,  $B_{high} = 4.068 T$ , OPERA currents  $I_{low} = 94.3 A$ ,  $I_{high} = 322.7 A$ .

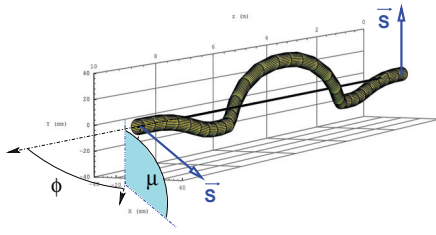


Figure 7: Helical orbit and spin rotation across a snake ( $\vec{S}$  rotation by RHIC full snake is  $\mu = 180^\circ$ , around an apparent rotation direction at  $\phi = \pm 45^\circ$  to the helix axis).

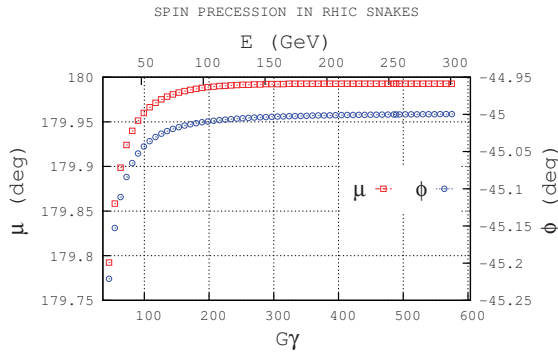


Figure 8: Energy dependence of the spin rotation angle  $\mu$ , and rotation axis orientation  $\phi$ .

### IN RHIC

Some aspects of the optics and polarization have been re-visited using the OPERA field maps of the snakes in Blue and Yellow RHIC rings models. Parameters so obtained assume a defect-free ring and include the separation bumps at IPs. They are briefly summarized hereafter (Figs. 9-11 and Tab. 1)

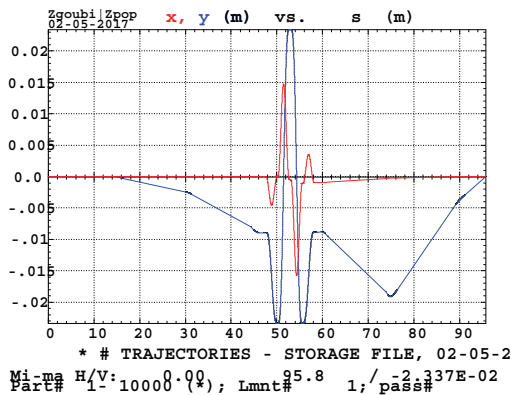


Figure 9: Left: H and V orbits in snake bump region, at injection. Right: orbits in RHIC including snake bumps.

The spin rotation by the snake may slightly depart from  $180^\circ$  (under the effects of the orbit bumps at the snakes, or the energy-dependence of  $\mu$  and  $\phi$ ) thus the periodic spin precession axis  $\vec{n}_0(s)$  is not exactly vertical, Fig. 11.

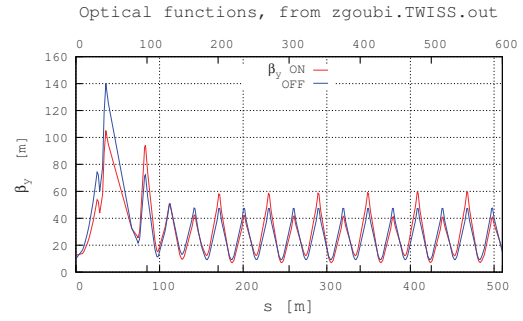


Figure 10: IP6-IP8 region of vertical optical functions in RHIC at injection, snakes ON or OFF. The overall effect is  $\Delta Q_y = +0.06$  with the snakes (Tab. 1).

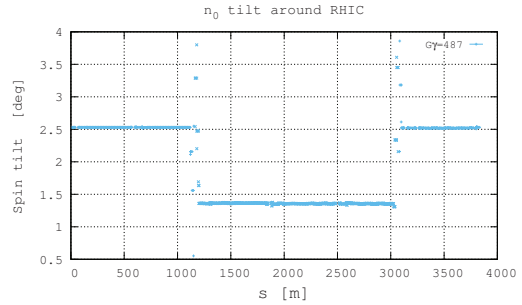


Figure 11: Deviation of the periodic spin precession axis  $\vec{n}_0$  from the vertical, around RHIC. The discontinuities are at the snakes.

Table 1: Optical Parameters and Spin Tune, at Injection and at Store, w/ and w/o Snakes

	$Q_x/Q_y$	$\xi_x/\xi_y$	$Q_s$
<b>Injection</b>			
no snakes	28.69 / 29.68	52 / 54	
w/ snakes	28.68 / 29.74	52 / 54	0.49987
<b>255 GeV, w/o [or w/] snakes</b>	28.685 / 29.675[5]	2.1 / 2.1[.3]	0.50000

### REFERENCES

- [1] F. Méot *et al.*, Exploring a Possible Origin of an Abnormal 10 ~ 15 degree Spin Tilt Observed at RHIC Polarimeters, *SPIN'16 Conf.*, Champaign, IL, USA.
- [2] W. W. MacKay *et al.*, Spin dynamics in AGS and RHIC, *PAC 2003*.
- [3] M. Anerella *et al.*, Helical Magnets, in *The RHIC Magnet System, Nuclear Instrum. Meth. A 499 (2003) 280-315*.
- [4] E. Courant, Hybrid helical snakes and rotators for RHIC, Spin Note SN10 (Jan. 1996).
- [5] W. MacKay, Path Length through Helical Snakes and Rotators, Tech Note BNL C-A/AP/140 (2004).
- [6] T. Roser *et al.*, Helical Partial Snakes for the AGS, AGS/RHIC/SN 072
- [7] Y.A. anferov, Helical snakes with no orbit correction and their discrete analogues, *Part. Acc.* Vol. 48, pp. 61-73 (1994).

- [8] M. Okamura, Three dimensional field analysis of helical snake magnets for RHIC, AGS/RHIC/SN 030 (June. 1996).
- [9] A. Luccio, Optimization of spin angles from a helix field map, AGS/RHIC/SN 042 (Nov. 1996).
- [10] F. Méot, Zgoubi Users' Guide, Tech. Note CA-AP/ (2012), Rep. BNL-98726-2012-IR.